Journal of Solid State Chemistry 182 (2009) 2417–2422

Contents lists available at ScienceDirect

Journal of Solid State Chemistry

journal homepage: www.elsevier.com/locate/jssc

Eu*T*Zn (T = Pd, Pt, Au) with TiNiSi-type structure—Magnetic properties and ^{151}Eu Mössbauer spectroscopy

Trinath Mishra, Wilfried Hermes, Thomas Harmening, Matthias Eul, Rainer Pöttgen *

Institut für Anorganische und Analytische Chemie and NRW Graduate School of Chemistry, Westfälische Wilhelms-Universität Münster, Corrensstrasse 30, 48149 Münster, Germany

ARTICLE INFO

Article history:
Received 15 May 2009
Received in revised form
15 June 2009
Accepted 21 June 2009
Available online 27 June 2009

Keywords:
Intermetallic compounds
Crystal chemistry
Europium
Magnetic properties
Mössbauer spectroscopy

ABSTRACT

The europium compounds Eu*T*Zn (T = Pd, Pt, Au) were synthesized from the elements in sealed tantalum tubes in an induction furnace. These intermetallics crystallize with the orthorhombic TiNiSi-type structure, space group *Pnma*. The structures were investigated by X-ray diffraction on powders and single crystals: $a = 732.3(2)$, $b = 448.5(2)$, $c = 787.7(2)$ pm, $R_1/wR_2 = 0.0400/0.0594$, 565 F^2 values for EuPdZn, $a = 727.8(3)$, $b = 443.7(1)$, $c = 781.7(3)$ pm, $R_1/wR_2 = 0.0605/0.0866$, 573 F^2 values for EuPtZn, and $a = 747.4(2)$, $b = 465.8(2)$, $c = 789.1(4)$ pm, $R_1/wR_2 = 0.0351/0.0590$, 658 F^2 values for EuAuZn, with 20 variables per refinement. Together the *T* and zinc atoms build up three-dimensional [*T*Zn] networks with short *T*–Zn distances. The Eu*T*Zn compounds show Curie–Weiss behavior in the temperature range from 75 to 300 K with $\mu_{eff} = 7.97(1)$, 7.70(1), and 7.94(1) μ_B/Eu atom and $\theta_P = 18.6(1)$, 34.9(1), and 55.5(1) K for T = Pd, Pt, and Au, respectively, indicating divalent europium. Antiferromagntic ordering was detected at 15.1(3) K for EuPdZn and canted ferromagnetic ordering at 21.2(3) and 51.1(3) K for EuPtZn and EuAuZn. ^{151}Eu Mössbauer spectroscopic measurements confirm the divalent nature of the europium atoms by isomer shift values ranging from −8.22(8) (EuPtZn) to −9.23(2) mm/s (EuAuZn). At 4.2 K full magnetic hyperfine field splitting is observed in all three compounds due to magnetic ordering of the europium magnetic moments.

1. Introduction

Most equiatomic *RETX* compounds (*RE* = rare-earth element; T = late transition metal; X = element of the 3rd, 4th, or 5th main group) have a common structural motif. The rare-earth elements as the most electropositive component transfer electron density to the *T* and *X* atoms, enabling covalent *T*–*X* bonding. Consequently, the *T* and *X* atoms build up two- or three-dimensional $[TX]^{\delta-}$ polyanionic networks, which are charge-compensated by $RE^{\delta+}$. The latter either separate the two-dimensional networks or fill channels and/or cages in the three-dimensional ones. Although the *RETX* compounds crystallize with more than 30 different structure types [1], several of them are closely related and derive from the AlB_2 type [2].

Recently it was shown, that the *p* element of the $[TX]^{\delta-}$ polyanions can also be replaced by magnesium, cadmium, or zinc, leading to substantial covalent *T*–Mg, *T*–Cd, and *T*–Zn bonding. To date, only few *RETZn* compounds have been reported, i.e. *RE*NiZn (*RE* = La–Pr, Sm, Gd, Dy, Er) [3,4], *RE*CuZn (*RE* = Y, La–Pr, Sm, Gd, Dy, Er, Yb) [5,6], *RE*RhZn (*RE* = Y, La–Nd, Sm, Gd–Lu) [7,8], *RE*PdZn (*RE* = Ce, Pr, Sm, Gd, Dy, Er, Yb) [3,9,10], *RE*AgZn (*RE* = Y, La–Nd, Sm, Gd, Er, Yb) [6], *RE*PtZn (*RE* = Ce, Yb, Lu) [9,11,12], and *RE*AuZn (*RE* = Ce, Yb) [4,9]. These *RETZn* compounds crystallize with three different structure types: TiNiSi (*Pnma*), LaNiAl (*Pnma*), or ZrNiAl ($P\bar{6}2m$), similar to their counterparts with a *p* element.

Several *RETZn* compounds have been studied with respect to their interesting magnetic properties. YbPtZn [9] contains trivalent ytterbium and shows magnetic ordering at 1.35 K. In contrast, YbAuZn and YbPdZn contain divalent ytterbium, similar to LuPtZn, and these compounds are Pauli paramagnets and metallic conductors. The two modifications of CePdZn [10] are paramagnetic with purely trivalent cerium. β-CePdZn orders antiferromagnetically at 3.2(1) K. This is also the case for the dense Kondo system CePtZn [11,12], which shows antiferromagnetic ordering at 1.7 K.

In continuation of our systematic studies on equiatomic europium compounds [13–17, and references therein], we were interested in the corresponding Eu*T*Zn phases. Recent phase analytical investigations in the Eu–*T*–Zn systems revealed the new phases EuPdZn, EuPtZn, and EuAuZn with TiNiSi type. The structure refinements and magnetic properties of these new compounds are reported herein.

2. Experimental

2.1. Synthesis

Starting materials for the preparation of Eu*T*Zn (T = Pd, Pt, Au) were sublimed ingots of europium (Johnson Matthey), palladium

* Corresponding author. Fax: +49 251 83 36002.
E-mail address: pottgen@uni-muenster.de (R. Pöttgen).

0022-4596/$ - see front matter © 2009 Elsevier Inc. All rights reserved.
doi:10.1016/j.jssc.2009.06.034

and platinum powder (Degussa-Hüls, ca. 200 mesh), gold wire (Degussa-Hüls, ∅ 1 mm) and zinc granules (Merck), all with stated purities better than 99.9%. The air- and moisture-sensitive europium ingots were kept in Schlenk tubes under dry argon prior to the reaction. Argon was purified with titanium sponge (900 K), silica gel, and molecular sieves. The elements were weighed in the ideal atomic ratio and sealed in tantalum ampoules under an argon pressure of 800 mbar in an arc-melting apparatus [18]. The tantalum ampoules were subsequently placed in the water-cooled sample chamber of an induction furnace [19] (Hüttinger Elektronik, Freiburg, Germany, Typ TIG 2.5/300), heated to 1500 K, and kept at that temperature for 30 min. Finally, the temperature was lowered to 900 K, and the samples were annealed at that temperature for another 4 h and then cooled within the furnace after the power was switched off. The temperature was controlled by a Sensor Therm Methis MS09 pyrometer with an accuracy of ±30 K. No reaction with the container material was observed. The compact light-gray pieces and the dark-gray powders were stable in air.

2.2. EDX analyses

The phase purity of the bulk samples and of the single crystals of Eu*T*Zn (T = Pd, Pt, Au) investigated on the diffractometers was analyzed using a Leica 420I scanning electron microscope. EuF_3, Pt, Pd, Au, and Zn were used as standards for semiquantitative EDX analysis. No impurity elements heavier than sodium were observed. The experimentally determined compositions were very close to the ideal one.

2.3. X-ray image plate data and data collection

The polycrystalline Eu*T*Zn (T = Pd, Pt, Au) samples were analyzed by powder X-ray diffraction on a Guinier camera (equipped with an image plate system Fujifilm, BAS-1800) using Cu $K\alpha_1$ radiation and α-quartz (a = 491.30, c = 540.46 pm) as an internal standard. The orthorhombic lattice parameters (Table 1) were obtained from least-squares refinements of the powder data. The correct indexing of the diffraction lines was ensured by intensity calculations [20] using the positional parameters obtained from the structure refinements.

Irregularly shaped crystal fragments of Eu*T*Zn (T = Pd, Pt, Au) were obtained from the samples annealed in the induction furnace by mechanical fragmentation. The crystals were glued to quartz fibers using bees wax and were investigated by Laue photographs on a Buerger camera (white molybdenum radiation, image plate technique, Fujifilm, BAS-1800) in order to check the quality for intensity data collection. Intensity data of Eu*T*Zn (T = Pd, Pt, Au) were collected at room temperature using a four-circle diffractometer (CAD4) with graphite monochromatized Mo-$K\alpha$ (71.073 pm) or monochromatized Ag-$K\alpha$ (56.083 pm) radiation and a scintillation counter with pulse height discrimination. Scans were taken in the $\omega/2\theta$ mode. Empirical absorption corrections were applied on the basis of Ψ-scan data, accompanied by spherical absorption corrections. Details of data collections and structure refinements are listed in Table 1.

2.4. Physical properties measurements

The samples were packed in kapton foil and attached to the sample holder rod of a VSM for measuring the magnetic properties in a Quantum Design Physical-Property-Measurement-System in the temperature range 2.1–305 K with magnetic flux densities up to 80 kOe. For heat capacity (C_p) measurements (2.1–300 K) the samples were glued to the platform of a pre-calibrated heat capacity puck using *Apiezon N grease*.

2.5. Mössbauer spectroscopy

The 21.53 keV transition of ^{151}Eu with an activity of 130 MBq (2% of the total activity of a ^{151}Sm:EuF_3 source) was used for the ^{151}Eu Mössbauer spectroscopic experiments. The measurements were performed in the usual transmission geometry in commercial helium bath and flow cryostats. The temperature of the absorber could be varied from 4.2 to 300 K. The source was kept at room temperature in all experiments. The samples were placed

Table 1
Crystal data and refinement for Eu*T*Zn (T = Pd, Pt, Au) with TiNiSi structure type, space group *Pnma* (no. 62), Z = 4.

Empirical formula	EuPdZn	EuPtZn	EuAuZn
Molar mass	323.73 g/mol	412.42 g/mol	414.30 g/mol
Unit cell dimensions	a = 732.3(2) pm	a = 727.8(3) pm	a = 747.4(2) pm
(Guinier powder data)	b = 448.5(2) pm	b = 443.7(1) pm	b = 465.8(2) pm
	c = 787.7(2) pm	c = 781.7(3) pm	c = 789.1(4) pm
	V = 0.2587 nm^3	V = 0.2524 nm^3	V = 0.2747 nm^3
Calculated density	8.31 g/cm^3	10.85 g/cm^3	10.02 g/cm^3
Crystal size	20 × 20 × 60 μm^3	20 × 20 × 60 μm^3	20 × 20 × 40 μm^3
Wave length	Ag-$K\alpha$ (56.083 pm)	Ag-$K\alpha$ (56.083 pm)	Mo-$K\alpha$ (71.073 pm)
Transm. ratio (max/min)	1.49	3.10	2.01
Absorption coefficient	21.0 mm^{-1}	47.8 mm^{-1}	84.1 mm^{-1}
F(0 0 0)	556	684	688
θ range	3–26°	3–27°	3–35°
Range in $h\,k\,l$	±11, ±6, −12/+6	±11, ±6, ±12	±12, ±7, ±12
Total no. reflections	3121	3806	4484
Independent reflections	565 (R_{int} = 0.0521)	573 (R_{int} = 0.1323)	658 (R_{int} = 0.1474)
Reflections with $I \geq 2\sigma(I)$	453 (R_σ = 0.0304)	450 (R_σ = 0.0595)	583 (R_σ = 0.0682)
Data/parameters	565/20	573/20	658/20
Goodness-of-fit on F^2	1.026	1.088	1.130
Final R indices [$I \geq 2\sigma(I)$]	R_1 = 0.0262	R_1 = 0.0408	R_1 = 0.0280
	wR_2 = 0.0551	wR_2 = 0.0807	wR_2 = 0.0567
R indices (all data)	R_1 = 0.0400	R_1 = 0.0605	R_1 = 0.0351
	wR_2 = 0.0594	wR_2 = 0.0866	wR_2 = 0.0590
Extinction coefficient	0.0068(7)	0.0089(9)	0.0113(6)
Largest diff. peak and hole	1.80/−2.44 e/Å^3	4.58/−4.24 e/Å^3	3.07/−4.83 e/Å^3

within thin-walled PVC containers at a thickness corresponding to about 10 mg Eu/cm^2.

3. Results and discussion

3.1. Structure refinements

The diffractometer data sets of three Eu*T*Zn compounds showed primitive orthorhombic cells and the systematic extinctions were compatible with space groups *Pnma* (TiNiSi type [21]) similar to our recent investigations on isotypic EuAuMg [22] and EuAgMg [23]. The atomic parameters of EuAuMg [22] were taken as starting parameters and the structures were refined using SHELXL-97 [24] (full-matrix least-squares on F^2) with anisotropic atomic displacement parameters for all atoms. As a check for the correct composition, the occupancy parameters were refined in a separate series of least-squares cycles. All sites were fully occupied within two standard uncertainties and in the final cycles the ideal occupancies were assumed again. The positional parameters and interatomic distances are listed in Tables 2 and 3.

Further details on the structure refinements are available from Fachinformationszentrum Karlsruhe, D-76344 Eggenstein-Leopoldshafen (Germany), by quoting Registry nos. CSD–420683 (EuPdZn), CSD–420684 (EuPtZn), and CSD–420674 (EuAuZn).

3.2. Crystal chemistry

New compounds Eu*T*Zn crystallize with the orthorhombic TiNiSi-type structure [21], space group *Pnma*. The transition elements have distorted tetrahedral zinc coordination at *T*–Zn distances ranging from 266 to 271 pm (T = Pd), 264–271 pm (T = Pt) and 271–283 pm (T = Au), somewhat longer than the sum of the covalent radii of 253, 254, and 259 pm, respectively [25]. These tetrahedra are condensed via all corners leading to a three-dimensional [*T*Zn] network in which the europium atoms fill channels. Since the crystal chemistry and chemical bonding of TiNiSi-type compounds have intensively been discussed in various review articles [2,26–29], herein we focus only on the structural peculiarities of the Eu*T*Zn series with respect to the change of the Eu coordination sphere caused by *T*.

Fig. 1 shows the coordination polyhedra of the Eu atoms in the three compounds. Since palladium and platinum have a similar covalent radius of 128 and 129 pm [25], there is no significant change in the coordination of the Eu atoms between EuPdZn and EuPtZn. Moving on to EuAuZn, the most significant difference is the distances between the Eu atoms. In the case of T = Pd and Pt the distances range from 373 to 378 pm, while with T = Au the Eu–Eu distances range from 383 to 390 pm. Furthermore, the course of the interatomic distances (Table 3) results in a different puckering of the [*T*Zn] network for EuAuZn and therefore a slightly different connection of the Eu atoms to the [*T*Zn] network, as compared to EuPdZn and EuPtZn.

Table 2
Atomic positions and anisotropic displacement parameters (pm^2) of Eu*T*Zn (T = Pd, Pt, Au), space group *Pnma*.

Atom	x	z	U_{11}	U_{22}	U_{33}	U_{13}	U_{eq}
EuPdZn							
Eu	0.01259(5)	0.69268(6)	114(2)	118(2)	126(2)	−6(1)	119(1)
Pd	0.29479(9)	0.39891(9)	156(3)	110(3)	150(3)	16(2)	139(2)
Zn	0.66246(13)	0.42312(13)	165(4)	131(5)	132(5)	−15(4)	142(2)
EuPtZn							
Eu	0.01176(11)	0.69132(11)	113(4)	122(4)	133(3)	−5(3)	123(2)
Pt	0.29092(8)	0.39782(9)	120(3)	114(3)	144(3)	10(2)	126(2)
Zn	0.6615(3)	0.4235(2)	142(8)	104(9)	133(9)	−26(6)	126(4)
EuAuZn							
Eu	0.00538(5)	0.69792(5)	46(2)	115(3)	103(2)	−7(1)	88(1)
Au	0.29698(5)	0.40667(4)	83(2)	103(2)	115(1)	14(1)	100(1)
Zn	0.67498(16)	0.42050(12)	105(5)	117(6)	106(4)	−12(3)	109(2)

All atoms lie on Wyckoff sites 4*c* (x 1/4 z).
The anisotropic displacement factor exponent takes the form: $-2\pi^2[(ha^*)^2U_{11}+\cdots+2hka^*b^*U_{12}]$; $U_{12}=U_{23}=0$; U_{eq} is defined as one third of the trace of the orthogonalized U_{ij} tensor.

Table 3
Interatomic distances (pm) for Eu*T*Zn (T = Pd, Pt, Au)[a].

		EuPdZn	EuPtZn	EuAuZn
Eu				
1	*T*	310.3	306.5	316.7
2	*T*	310.8	309.7	321.2
2	Zn	316.3	313.1	321.3
1	Zn	322.4	320.2	326.7
1	Zn	331.9	329.9	330.0
2	*T*	325.8	320.3	334.9
2	Zn	338.5	337.4	346.5
1	*T*	359.1	359.1	348.7
2	Eu	377.1	372.8	382.6
2	Eu	377.9	375.3	389.7
T				
2	Zn	266.2	264.4	270.7
1	Zn	271.1	268.2	273.8
1	Zn	271.2	270.5	282.7
1	Eu	310.3	306.5	316.7
2	Eu	310.8	309.7	321.2
2	Eu	325.8	320.3	334.9
1	Eu	359.1	359.1	348.7
Zn				
2	*T*	266.2	264.5	270.7
1	*T*	271.1	268.2	273.8
1	*T*	271.2	270.5	282.7
2	Eu	316.3	313.1	321.3
1	Eu	322.4	320.2	326.7
1	Eu	331.9	329.9	330.0
2	Eu	338.5	337.4	346.5

[a] Standard deviations are all equal or less than 0.2 pm. All distances within the first coordination spheres are listed.

3.3. Physical properties

The temperature dependence of the magnetic ($\chi = M/H$) and the inverse magnetic susceptibility $\chi^{-1}(T)$ of Eu*T*Zn (T = Pd, Pt, Au) is displayed in Fig. 2, measured while warming in a *dc* field of 10 kOe in the case of EuPdZn and EuAuZn and 40 kOe for EuPtZn, after zero field cooling each sample to the lowest available temperature. For all compounds studied here, χ increases with decreasing temperature. We used a higher field for EuPtZn to saturate the small ferromagnetic anomaly of surface EuO at T_C = 69 K [30–32], which was seen while measuring with a field of 10 kOe.

All three compounds show Curie–Weiss behavior in the temperature range 75–300 K. A fit of the susceptibility data in this temperature range revealed the effective magnetic moments (μ_{eff}) and paramagnetic Curie temperatures (θ_P) given in Table 4. These μ_{eff} values are close to the free ion value of 7.94 μ_B for Eu^{2+}, thus indicating purely divalent europium. The θ_P values indicate that the magnetic interaction is of a ferromagnetic type. An antiferromagnetic anomaly at around 14.5(3) K is clearly visible for EuPdZn. The $\chi(T)$ data show ferromagnetic ordering around 26 K for EuPtZn and around 53 K for EuAuZn, a comparatively high ordering temperature.

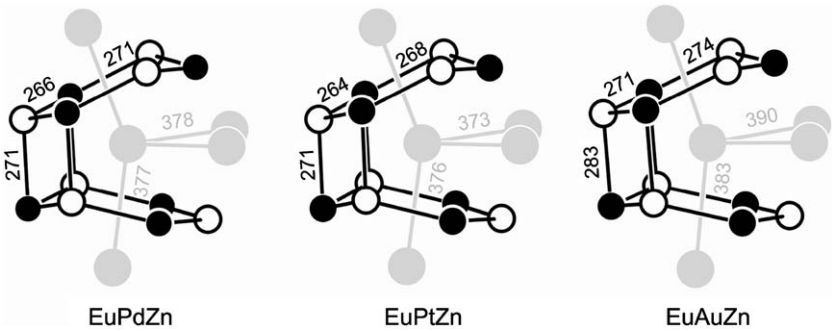

Fig. 1. Near-neighbor coordination of the Eu-atoms in Eu*T*Zn (T = Pd, Pt, Au). Eu, *T*, and Zn atoms are drawn as medium gray, black, and open circles, respectively. The puckered T_3Zn_3 hexagons are emphasized and relevant interatomic distances are indicated.

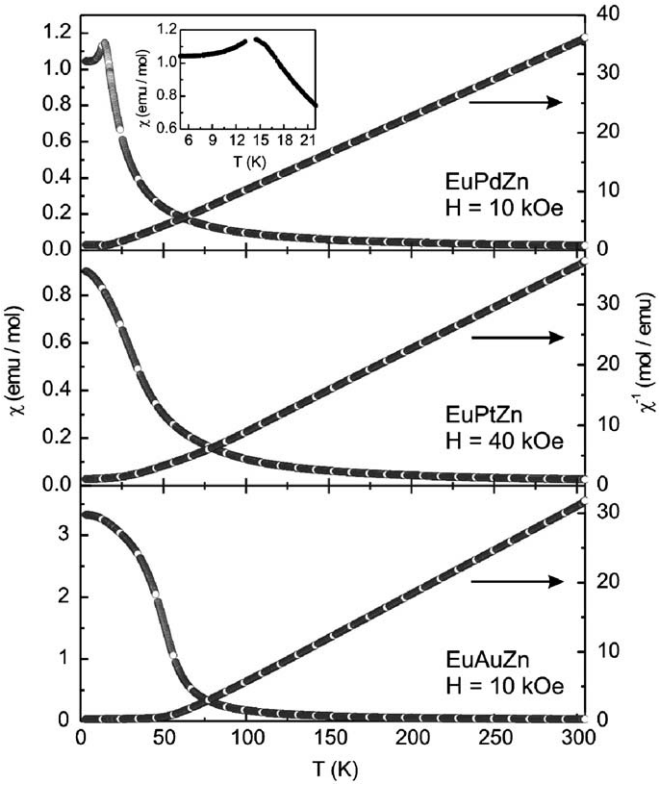

Fig. 2. Temperature dependence of the magnetic (χ) and the inverse magnetic susceptibility (χ^{-1}) of Eu*T*Zn (T = Pd, Pt, Au). The inset highlights the low-temperature behavior of EuPdZn.

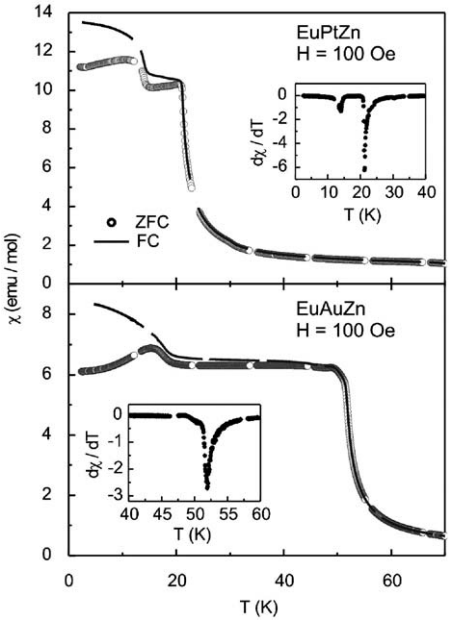

Fig. 3. Low-temperature susceptibility (zero field cooling and field cooling modus) of EuPtZn and EuAuZn at 100 Oe (kink-point measurement). The insets show the derivative $d\chi/dT$ of the field cooling curve with sharp peaks at the Curie temperatures.

Table 4
Effective magnetic moment (μ_{eff}, 75–300 K range), paramagnetic Curie temperature (θ_P), Néel temperature (T_N) and Curie temperature (T_C) from C_p data and the moment values at 80 kOe and 5 K ($\mu_{exp(m)}$).

Compound	μ_{eff} (μ_B/Eu atom)	θ_P (K)	T_N, T_C (K)	$\mu_{exp(m)}$ (μ_B/Eu atom)
EuPdZn	7.97(1)	18.6(1)	15.1(3)	6.94(1)
EuPtZn	7.70(1)	34.9(1)	21.2(3)	6.73(1)
EuAuZn	7.94(1)	55.5(1)	51.1(3)	6.86(1)

We have therefore measured the susceptibility in a low external field of 100 Oe in the zero field cooling and in the field cooling mode (Fig. 3). The derivative $d\chi/dT$ of the zero field cooling measurement resulted in Curie temperatures of T_C = 21.2(1) K for EuPtZn and 51.9(2) K for EuAuZn. With further decrease in temperature $\chi(T)$ in ZFC and FC modes continue almost independent of temperature down to 15 and 19 K (EuPtZn, EuAuZn). At this temperature both the ZFC and *FC* curves start to increase equally with decrease in temperature again, whereas at 15 and 12 K (EuAuZn, EuPtZn) we observe a strong bifurcation of ZFC and FC modes. This phenomenon can appear only if both compounds order as a canted ferromagnet at 21.2 and 51.9 K (EuPtZn, EuAuZn), so that there is a spin-reorientation at temperatures of 15 and 19 K. Thus, the spins move into a more parallel position.

In order to understand the nature of the magnetic ordering, we have obtained isothermal *M* (in ZFC mode) at selected temperatures below and above the transition temperatures up to 80 kOe (Fig. 4). At 50 K (75 K) we observe almost linear increase of the magnetization with the applied field as expected for a paramagnetic material. The magnetization isotherm of EuPdZn at 5 K increases linearly with increase in *H* up to a field strength of around 40 kOe and saturates to a value of about 6.94 μ_B/Eu atom

above 40 kOe, which is close to the expected value, $g_J \times S = 7\,\mu_B\,mol^{-1}$. This magnetization behavior is similar to EuPdIn [33].

In contrast, at 5 K the magnetization of EuPtZn and EuAuZn almost reaches saturation at external field strengths of 2 T and the saturation magnetizations (sm) at 80 kOe reach values given in Table 4, in good agreement with the theoretical value. Considering the very small hysteresis, EuPtZn and EuAuZn can be classified as soft and weak canted ferromagnets. In Fig. 5, the specific heat (C_P) data are plotted for Eu*T*Zn. The Néel and Curie temperatures given in Table 5 for Eu*T*Zn (T = Pd, Pt, Au) are characterized by a λ-like anomaly and are in line with the magnetic data. The data give no hint for the spin-reorientation as observed in $\chi(T)$ in the case of EuPtZn and EuAuZn, so it can only be considered as a weak effect for both cases.

EuPdZn, EuPtZn, and EuAuZn order magnetically at distinctly different temperatures. The latter, however, do not simply scale with the Eu–Eu distances. This is also the case for the many other Eu*TX* phases with TiNiSi-type structure or a related superstructure type [13]. A reason might be the differing tilt of the T_3X_3 hexagons (exemplarily shown for the Eu*T*Zn compounds in Fig. 1) around the europium atoms. However, a clear correlation exists between the valence electron concentration and the ^{151}Eu isomer shift (vide infra).

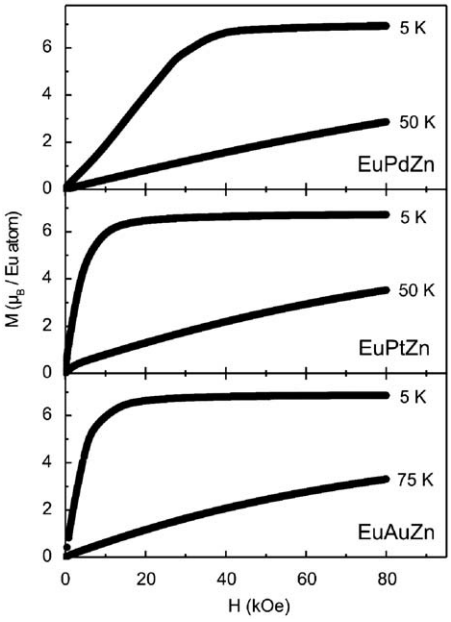

Fig. 4. Magnetization isotherms of Eu*T*Zn (T = Pd, Pt, Au).

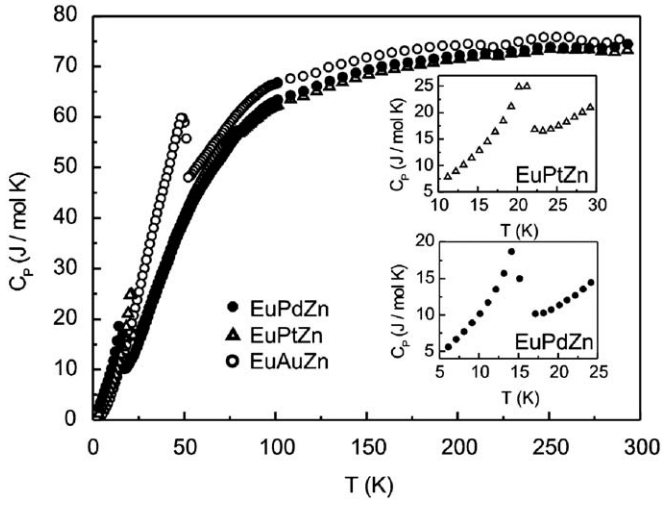

Fig. 5. Temperature dependence of the specific heat of Eu*T*Zn (T = Pd, Pt, Au) in zero magnetic field. The low-temperature behavior of EuPdZn and EuPtZn is shown in the insets.

3.4. Mössbauer spectroscopy

Experimental and simulated ^{151}Eu Mössbauer spectra of EuPdZn, EuPtZn and EuAuZn at 78 and 4.2 K are presented in Figs. 6 and 7, respectively. The corresponding fitting parameters are listed in Table 5. The spectra are composed of one major resonance at isomer shift values corresponding to divalent europium. The minor (~8% intensity) components in the zero velocity vicinity observed for EuPdZn and EuPtZn are attributed to extrinsic Eu^{3+}, formed due to surface oxidation during grinding. EuAuZn shows no Eu^{III} contamination. The ^{151}Eu isomer shift values obey the correlation reported in [34], thus decreasing with

Table 5
Fitting parameters for ^{151}Eu Mössbauer spectroscopic measurements on Eu*T*Zn (T = Pd, Pt, Au): isomer shift (δ_{iso}), electric quadrupole interaction (ΔE_Q), magnetic hyperfine field (B_{hf}), and experimental line width (Γ).

T (K)	δ_{iso} (mm/s)	Γ (mm/s)	ΔE_Q (mm/s)	B_{Hf} (T)
EuPdZn				
78	−8.48(4)	2.7(2)	2.6(6)	–
4.2	−8.28(2)	2.63(6)	1.0(1)	18.21(6)
EuPtZn				
78	−8.22(8)	2.38(3)	4.51(7)	–
4.2	−7.89(5)	2.5(1)	3.0(3)	22.0(2)
EuAuZn				
78	−9.23(2)	2.10(6)	3.9(1)	–
4.2	−8.82(4)	2.6(1)	−1.1(3)	17.8(1)

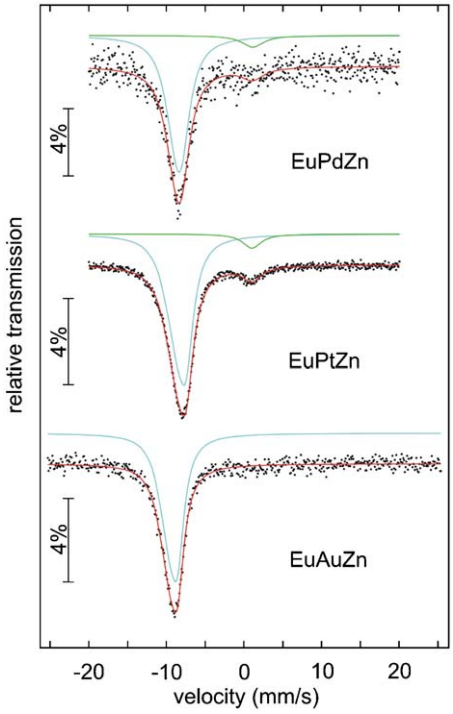

Fig. 6. Experimental and simulated ^{151}Eu Mössbauer spectra of Eu*T*Zn (T = Pd, Pt, Au) at 78 K.

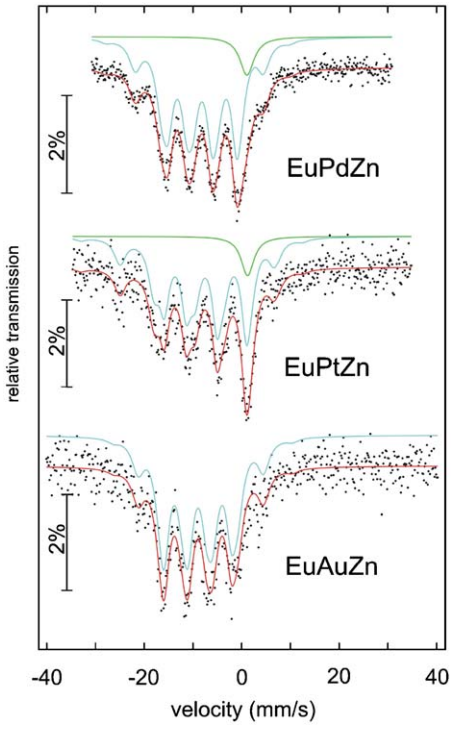

Fig. 7. Experimental and simulated ^{151}Eu Mössbauer spectra of Eu*T*Zn (T = Pd, Pt, Au) at 4.2 K.

increasing electron count. At 4.2 K the europium magnetic moments in all compounds are in ordered states (*vide infra*) leading to magnetic hyperfine fields of 18–22 T acting on the nuclear spin levels resulting in clearly visible Zeeman splittings.

Acknowledgments

This work was financially supported by the Deutsche Forschungsgemeinschaft. T.M., T.H., and W.H. are indebted to the NRW Graduate School of Chemistry and the Fonds der Chemischen Industrie for PhD stipends.

References

[1] M.L. Fornasini, F. Merlo, J. Alloys Compd. 219 (1995) 63.
[2] R.-D. Hoffmann, R. Pöttgen, Z. Kristallogr. 216 (2001) 127.
[3] A. Iandelli, J. Alloys Compd. 182 (1992) 87.
[4] W. Hermes, R. Mishra, U.Ch. Rodewald, R. Pöttgen, Z. Naturforsch. 63b (2008) 537.
[5] P. Morin, D. Gignoux, J. Voiron, A.P. Murani, Physica B 180–181 (1992) 173.
[6] M.L. Fornasini, A. Iandelli, F. Merlo, M. Pani, Intermetallics 8 (2000) 239.
[7] W. Hermes, A.F. Al Alam, S.F. Matar, R. Pöttgen, Solid State Sci. 10 (2008) 1895.
[8] W. Hermes, R. Pöttgen, Solid State Sci. 11 (2009) 706.
[9] S.K. Dhar, R. Kulkarni, P. Manfrinetti, M. Pani, Y. Yonezawa, Y. Aoki, Phys. Rev. B 76 (2007) 054411.
[10] W. Hermes, R. Mishra, H. Müller, D. Johrendt, R. Pöttgen, Z. Anorg. Allg. Chem. 635 (2009) 660.
[11] R. Mishra, W. Hermes, R. Pöttgen, Z. Naturforsch. 62b (2007) 1581.
[12] S.K. Dhar, R. Kulkarni, H. Hidaka, Y. Toda, H. Kotegawa, T.C. Kobayashi, P. Manfrinetti, A. Provino, J. Phys.: Condens. Matter 21 (2009) 156001.
[13] R. Pöttgen, D. Johrendt, Chem. Mater. 12 (2000) 875.
[14] R. Pöttgen, R.-D. Hoffmann, M.H. Möller, G. Kotzyba, B. Künnen, C. Rosenhahn, B.D. Mosel, J. Solid State Chem. 145 (1999) 174.
[15] R. Pöttgen, R.-D. Hoffmann, R. Müllmann, B.D. Mosel, G. Kotzyba, Chem. Eur. J. 3 (1997) 1852.
[16] D. Johrendt, G. Kotzyba, H. Trill, B.D. Mosel, H. Eckert, Th. Fickenscher, R. Pöttgen, J. Solid State Chem. 164 (2002) 201.
[17] R. Kraft, R.-D. Hoffmann, C.P. Sebastian, R. Pöttgen, Yu. Prots, W. Schnelle, M. Schmidt, Yu. Grin, Chem. Mater. 20 (2008) 1948.
[18] R. Pöttgen, Th. Gulden, A. Simon, GIT Labor Fachz. 43 (1999) 133.
[19] D. Kußmann, R.-D. Hoffmann, R. Pöttgen, Z. Anorg. Allg. Chem. 624 (1998) 1727.
[20] K. Yvon, W. Jeitschko, E. Parthé, J. Appl. Crystallogr. 10 (1977) 73.
[21] C.B. Shoemaker, D.P. Shoemaker, Acta Crystallogr. 18 (1965) 900.
[22] R. Pöttgen, R.-D. Hoffmann, J. Renger, U.Ch. Rodewald, M.H. Möller, Z. Anorg. Allg. Chem. 626 (2000) 2257.
[23] Th. Fickenscher, R. Pöttgen, J. Solid State Chem. 161 (2001) 67.
[24] G.M. Sheldrick, SHELXL-97—Program for Crystal Structure Refinement, University of Göttingen, Germany, 1997.
[25] J. Emsley, The Elements, Oxford University Press, Oxford, UK, 1999.
[26] G. Nuspl, K. Polborn, J. Evers, G.A. Landrum, R. Hoffmann, Inorg. Chem. 35 (1996) 6922.
[27] G.A. Landrum, R. Hoffmann, J. Evers, H. Boysen, Inorg. Chem. 37 (1998) 5754.
[28] M.D. Bojin, R. Hoffmann, Helv. Chim. Acta 86 (2003) 1653.
[29] E. Parthé, L. Gelato, B. Chabot, M. Penzo, K. Cenzual, R. Gladyshevskii, TYPIX–standardized data and crystal chemical characterization of inorganic structure types, in: Gmelin Handbook of Inorganic and Organometallic Chemistry, eighth ed., Springer, Berlin, Germany, 1993.
[30] B.T. Matthias, R.M. Bozorth, J.H. Van Vleck, Phys. Rev. Lett. 5 (1961) 160.
[31] D.B. McWhan, P.C. Souers, G. Jura, Phys. Rev. 143 (1966) 385.
[32] B. Stroka, J. Wosnitza, E. Scheer, H.v. Löhneysen, W. Park, K. Fischer, Z. Phys. B–Condens. Matter 89 (1992) 39.
[33] R. Pöttgen, J. Mater. Chem. 6 (1996) 63.
[34] R. Müllmann, U. Ernet, B.D. Mosel, H. Eckert, R.K. Kremer, R.-D. Hoffmann, R. Pöttgen, J. Mater. Chem. 11 (2001) 1133.